SIGNAL TRANSDUCTION

Evaluating biological activity of compounds by transcription factor activity profiling

Alexander Medvedev[1], Matt Moeser[1]*, Liubov Medvedeva[1], Elena Martsen[1], Alexander Granick[1], Lydia Raines[1], Ming Zeng[1], Sergei Makarov Jr.[1], Keith A. Houck[2], Sergei S. Makarov[1†]

Assessing the biological activity of compounds is an essential objective of biomedical research. We show that one can infer the bioactivity of compounds by assessing the activity of transcription factors (TFs) that regulate gene expression. Using a multiplex reporter system, the FACTORIAL, we characterized cell response to a compound by a quantitative signature, the TF activity profile (TFAP). We found that perturbagens of biological pathways elicited distinct TFAP signatures in human cells. Unexpectedly, perturbagens of the same pathway all produced identical TFAPs, regardless of where or how they interfered. We found invariant TFAPs for mitochondrial, histone deacetylase, and ubiquitin/proteasome pathway inhibitors; cytoskeleton disruptors; and DNA-damaging agents. Using these invariant signatures permitted straightforward identification of compounds with specified bioactivities among uncharacterized chemicals. Furthermore, this approach allowed us to assess the multiple bioactivities of polypharmacological drugs. Thus, TF activity profiling affords straightforward assessment of the bioactivity of compounds through the identification of perturbed biological pathways.

INTRODUCTION

To predict the therapeutic use and toxicity of a chemical, one must know its biological activity, which requires finding its targets within a living cell. This task is difficult because cells have myriads of components. Moreover, chemicals often interact with multiple targets. Transcriptomics has become a favorite strategy in conducting bioactivity assessments. The transcriptomics-based approaches characterize cell response to a compound by a "gene signature," representing a list of differentially expressed genes (*1*). Mapping the differential genes to Gene Ontology provides information about the affected biological processes. These approaches have been widely used to annotate the biological activity of drugs and environmental chemicals. However, "backtracking" of gene expression changes to the primary cause, that is, the biological pathways, requires complex computations and has met with limited success (*2*, *3*). Particularly challenging are the assessments of polypharmacological compounds that interact with multiple targets.

Here, we present an alternative approach to the identification of the biological activity of compounds that entails assessing responses of cellular signal transduction pathways that regulate gene expression. As a readout, we evaluate the activity of transcription factors (TFs) that connect the signaling pathways with the regulated genes. TFs are a class of proteins that bind specific sequences within the target genes, thereby modulating transcription. Thus, a TF activity profile (TFAP) captures the signals that regulate gene expression.

Many TF families that mediate cell responses to xenobiotics and various stress stimuli have been identified, but less is known about how an interplay of multiple TFs coordinates gene expression. As TF activity is regulated by various posttranslational modifications of preexistent TF proteins, TF activity may not correlate with TF protein content, hence the necessity to use functional TF assays, for example, reporter gene assays. However, conventional TF assays are not suited for the assessment of multiple TF responses. Therefore, we have developed a multiplex reporter system (the FACTORIAL) enabling a parallel assessment of the activity of multiple TFs in a single well of cells (*4*). We used this system to analyze TF responses to environmental chemicals and drugs (*5*, *6*).

Here, we used the FACTORIAL system to examine TF responses to perturbations of biological pathways and cell systems in human cells. Using this technology, we characterized cell response to a compound by a quantitative multi-endpoint signature, the TFAP. The assessment of a panel of landmark perturbagens revealed distinct TFAP signatures for the perturbed biological pathways and cell systems. Unexpectedly, we found that perturbagens of the same biological pathway all produced an invariant TFAP regardless of how and where they interfered. We show that these invariant TFAP signatures enabled straightforward identification of compounds with specified bioactivities among uncharacterized chemicals. We further show that examination of TFAP signatures of polypharmacological drugs enabled the identification of their on-target and off-target activities. In summary, this study demonstrates that TF activity profiling enables a straightforward assessment of the bioactivities of compounds through the identification of perturbed biological pathways.

RESULTS

Obtaining TFAP signatures by the FACTORIAL assay

Using the FACTORIAL assay, we obtained TFAP signatures for perturbagens of various cell systems and biological pathways in human cells. As described in our previous publication (*4*), the FACTORIAL reporter system comprises a set of TF-responsive reporter constructs called reporter transcription units (RTUs). Each RTU has a TF-specific promoter linked to a reporter sequence. When they are transfected into assay cells, the RTUs produce reporter RNAs proportionate to the activity of their promoters. Thus, we can assess the activity of TFs by profiling the reporter transcripts (Fig. 1A). Significantly, owing to a rapid turnover of reporter RNAs, this approach enables the detection of not only activated but also inhibited TFs.

To ensure equal detection efficacy for the TFs, we used a "homogeneous" detection approach. In this approach, all RTUs have identical

[1]Attagene Inc., P.O. Box 12054, Research Triangle Park, NC 27709, USA. [2]U.S. Environmental Protection Agency, 109 T.W. Alexander Drive, D343-03, Research Triangle Park, NC 27711, USA.
*Present address: Lineberger Cancer Research Center, University of North Carolina at Chapel Hill, Room 22-062, Chapel Hill, NC 27599–7295, USA.
†Corresponding author. Email: smak@attagene.com

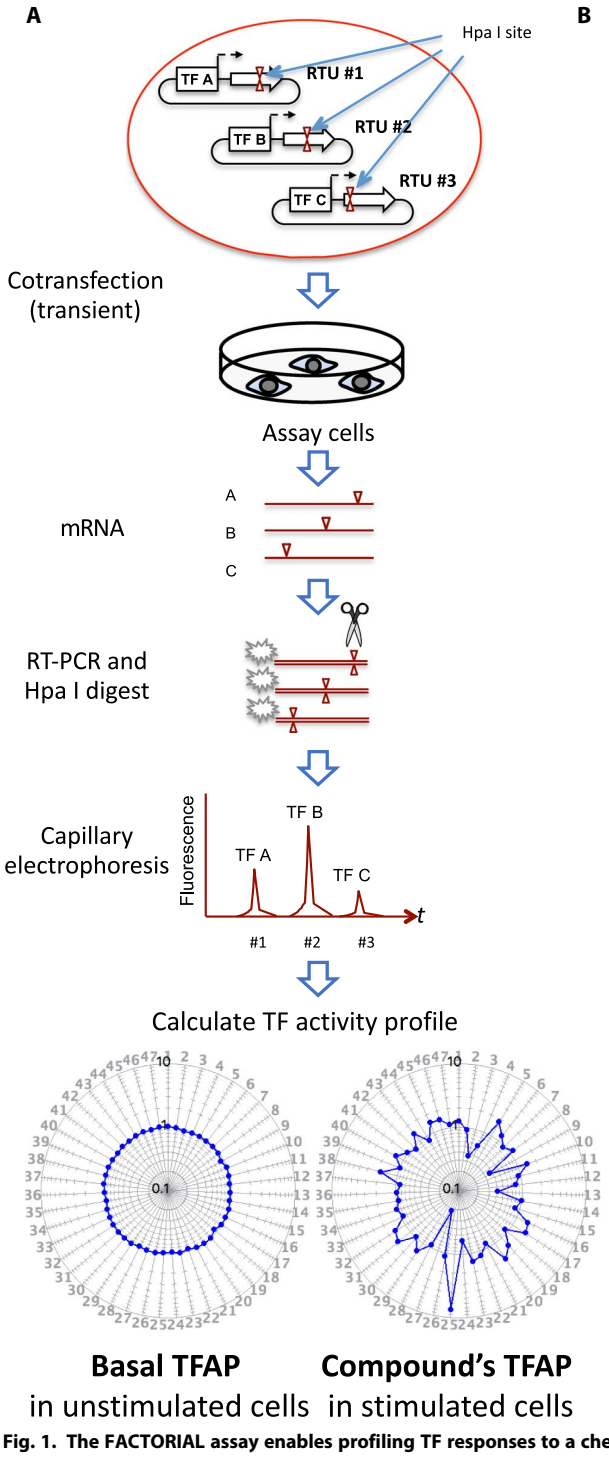

B

RTU #	Name	Transcription factor
1	TGFRE	TGF beta response element (SMAD3/4)
2	HNF6	Hepatocyte nuclear factor 6
3	TCF	TCF/LEF
4	Ebox	Myc and upstream stimulatory factor 1 (USF-1)
5	PPAR	Peroxisome proliferator activating receptor
6	NF1	Nuclear factor 1
7	GR	Glucocorticoid receptor
8	AP-1	Activator protein 1
9	ISRE	Interferon regulatory factors IRF1, IFR3
10	MTF-1	The metal regulatory transcription factor 1 (MTF-1)
11	STAT3	Signal transducer and activator of transcription 3
12	TAL	A minimal promoter
13	NF-κB	Nuclear factor kappa B
14	FoxA2	Forkhead box protein A2
15	CMV	Cytomegalovirus promoter-enhancer
16	Xbp1	X-box protein 1
17	CREB	cAMP-response element binding protein
18	AhR	Aryl hydrocarbon receptor
19	EGR	Early growth response protein 1
20	NRF2	Nuclear factor (erythroid-derived 2)-like 2
21	TA	A minimal promoter
22	ER	Estrogen receptor
23	Oct	Octamer transcription factor
24	LXR	Liver X receptor
25	HSF-1	Heat shock factor-1 protein
26	SREBP	Sterol regulatory element-binding protein
27	p53	The p53 transcription factor
28	BMPRE	Bone morphogenetic protein response element (SMAD4/5)
29	Pax6	Transcription factor paired box 6
30	HIF-1α	Hypoxia-inducible factor-1 alpha
31	VDR	Vitamin D receptor
32	ROR	Retinoic acid receptor-related orphan receptor protein
33	Ets	E-twenty six transcription factor
34	GLI-1	Gli-1 transcription factor
35	NRF1	Nuclear respiratory factor 1
36	GATA	GATA transcription factor
37	E2F	E2F transcription factor
38	C/EBP	The CCAAT-enhancer-binding protein
39	Myb	Transcriptional activator Myb
40	PBREM	Phenobarbital responsive enhancer module /constitutive androstane receptor
41	FXR	Farnesoid X receptor
42	AP-2	Activating protein 2
43	RAR	Retinoic acid receptor
44	FoxO	Forkhead box proteins FOXO1 and FOXO3
45	SOX	SOX transcription factor
46	Sp1	Sp1 transcription factor
47	Myc	Myc transcription factor

Fig. 1. The FACTORIAL assay enables profiling TF responses to a chemical. (**A**) Flowchart of the FACTORIAL assay. The assay cells were transiently transfected with a mix of 47 TF-specific RTUs. The RTUs contained a restriction tag (the Hpa I site) placed at different positions within the reporter sequences. The total RNA was amplified by RT-PCR, using a common pair of primers. The PCR products were labeled with a fluorescent label, digested by the Hpa I enzyme, and resolved by CE. The CE fluorescence profile reflected the activity of the TFs. The differential TFAP for a chemical shows changes in TF activity in the chemical-treated versus vehicle-treated cells. By this definition, the basal TFAP (in vehicle-treated cells) is a circle with $R = 1.0$. (**B**) TF endpoints of the FACTORIAL assay.

reporter sequences tagged by a unique endonuclease site (Hpa I) at a distinct position. The detection process entails reverse transcription polymerase chain reaction (RT-PCR) amplification of the reporter transcripts, followed by fluorescent labeling and Hpa I restriction. The labeled DNA fragments of predefined length are resolved by capillary electrophoresis (CE), producing a fluorescence profile that provides information about the activity of RTUs (Fig. 1A). The homogeneous detection approach enables robust and reproducible TF assessments (*4*).

The FACTORIAL assay used here was composed of 47 RTUs for TFs that mediate responses to a variety of stress stimuli and xenobiotics,

including nuclear factor κB (NF-κB), p53, AP-1, hypoxia-inducible factor–1a (HIF-1a), heat shock factor–1 (HSF-1), and many others (Fig. 1B). The RTU promoters contained one or multiple copies of TF binding sites for specified TF families. The reporter system also contained RTUs with minimal TATA and TAL promoters and cytomegalovirus (CMV) promoter.

Because chemicals have different cellular pharmacokinetics, we obtained the TFAP signatures after a prolonged (24-hour) exposure. We present these TFAP signatures in a radial graph format with 47 axes showing the stimulus-induced TF activity changes. By the definition, the baseline TFAP in unstimulated cells is a perfect circle with $R = 1.0$ (Fig. 1A). To assess the pairwise similarity of TFAPs, we used the Pearson correlation coefficient (*4*). The probability that two random 47-endpoint signatures have a similarity of $r > 0.7$ is less than 10^{-7} (*7*); thus, we presumed that two compounds elicited identical responses if their signatures' similarity was greater than 0.7.

The invariant TFAP of mitochondria inhibitors

In one set of experiments, we assessed TFAPs for inhibitors of the mitochondrial electron transport chain (mETC) in human hepatocytic HepG2 cells. The mETC comprises functionally linked protein complexes within the internal mitochondrial membrane that transfer electrons from electron donors to oxygen. This process creates a proton gradient on the membrane that is converted into adenosine 5′-triphosphate (ATP) production. We evaluated a panel of specific inhibitors of different mETC complexes, including rotenone, pyridaben, and fenpyroximate (complex I inhibitors); antimycin A (a complex III inhibitor); and an ionophore valinomycin. We assessed these chemicals at multiple concentrations. To compare multiple TFAPs, we developed a clustering algorithm that calculated an average (consensus) signature for the multiple TFAPs (see Materials and Methods). The clustering of TFAPs of mETC inhibitors revealed a single cluster. The consensus signature had high similarity ($r \geq 0.8$) with the TFAPs of individual mETC inhibitors in a broad range of concentrations (Fig. 2A; for an alternative presentation of the TFAPs, see the heatmap in fig. S6). The consensus mETC TFAP comprised multiple TF responses, including activation of oxidative stress–responsive nuclear factor, erythroid 2-like 2 (NRF2)/antioxidant response element (ARE), which was consistent with published data (*8*).

HepG2 cells produce sufficient amounts of ATP via glycolysis to survive fully anaerobic conditions (*9*), and none of the mETC inhibitors caused cell death (fig. S1). Therefore, mETC perturbagens produced an invariant TFAP signature irrespective of their structural dissimilarity and their targets within the pathway.

The invariant TFAP of inhibitors of the ubiquitin/proteasome protein degradation pathway

The ubiquitin (Ub)/proteasome pathway (UPP) carries out the regulated degradation of cellular proteins (*10*). This process involves a consecutive action of a Ub-activating enzyme (E1), a Ub-conjugating enzyme (E2), and a substrate-specific Ub ligase (E3) that attaches Ub residues to substrate proteins, targeting them for degradation by the 26*S* proteasome (PS) (*10*). Using the FACTORIAL assay in HepG2 cells, we obtained TFAPs for a panel of chemicals specifically inhibiting different nodes of the UPP. Those included PYR-41 (an E1 inhibitor with no activity at E2), NSC 697923 (a selective inhibitor of the E2 Ub-conjugating enzyme UBE2N), deubiquitinase inhibitors b-AP15 and WP1130, and five PS inhibitors, including lactacystin (an organic compound naturally synthesized by *Streptomyces* bacteria), peptide aldehydes MG132 and PSI, a boronic chalcone derivative (AM114), and a peptide boronate (bortezomib).

Clustering these signatures revealed a single cluster with a consensus TFAP signature that had high similarity ($r \geq 0.7$) with the TFAPs of individual UPP inhibitors in a broad range of concentrations (Fig. 2B). The consensus TFAP comprised multiple TF responses, including activation of HSF-1 and NRF2/ARE RTUs and inhibition of the NF-κB RTU, which were in agreement with published data (*11*, *12*). Representative signatures of the UPP perturbagens are also shown as a heatmap in fig. S6.

As UPP inhibitors can cause cell death, we monitored cell viability. At the end of 24 hours of incubation and the concentrations used, none of the UPP inhibitors caused cell death. Some UPP inhibitors induced cell death after a prolonged (48-hour) incubation (fig. S2A). Thus, the invariant TFAP of UPP inhibitors cannot be explained by cell death.

The FACTORIAL assay in other cell types [mammary epithelial MCF-7 and kidney epithelial human embryonic kidney (HEK) 293 cells] showed that different UPP inhibitors also produced common, yet cell type–specific, TFAP signatures (fig. S2B). The common TF responses that were observed in all cell types were the activation of HSF-1 and NRF2/ARE RTUs, while other TF responses varied among cell lines. Therefore, different UPP perturbagens produced invariant TFAP signatures in different cell types, irrespective of the perturbagens' structure, their targets within the pathway, and their effects on cell viability.

The invariant TFAP of HDAC inhibitors

The enzyme families of histone acetyltransferases (HATs) and histone deacetylases (HDACs) catalyze the acetylation/deacetylation of histones and cellular proteins, which alters gene expression (*13*). Using the FACTORIAL assay in HepG2 cells, we evaluated a panel of structurally diverse HDAC inhibitors, including suberoylanilide hydroxamic acid, suberohydroxamic acid, CAY10398, M344, oxamflatin, pyroxamide, the cyclic peptide apicidin, and the mercaptoketone-based KD5170 (*14*). The clustering revealed a single TFAP cluster with a consensus TFAP that had high similarity ($r \geq 0.8$) with the TFAPs of individual HDAC inhibitors at multiple concentrations (Fig. 3A). Representative TFAPs for HDAC inhibitors are also shown in the fig. S6 heatmap.

The FACTORIAL assay in HEK293 and MCF-7 cells also revealed common, albeit cell type–specific, signatures of HDAC inhibitors in these cells (fig. S3A). After a 24-hour incubation, none of the HDAC inhibitors caused cell death (fig. S3B). Thus, structurally dissimilar HDAC inhibitors produced invariant TFAPs.

The invariant TFAP of cytoskeleton disruptors

Microtubules are tubular polymers of tubulin that, along with microfilaments and intermediate filaments, constitute the cytoskeleton of eukaryotic cells. Microtubules are dynamic structures whose length is regulated by the polymerization and depolymerization of tubulin (*15*). Using the FACTORIAL assay in HepG2 cells, we evaluated a panel of structurally dissimilar microtubule polymerization disruptors (MTDs), including colchicine, nocodazole, vinblastine, vincristine, and vinorelbine. Cluster analysis revealed a single cluster with a consensus TFAP signature that had high similarity to the TFAPs of individual MTDs at multiple concentrations ($r \geq 0.8$; Fig. 3B). The most prominent TF responses of the consensus TFAP were an up-regulation of AP-1 and CMV RTUs and down-regulation of T cell factor (TCF)/β-catenin and estrogen response element RTUs. These responses were

A Mitochondria ETC inhibitors

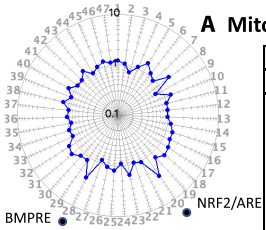

Consensus TFAP

Perturbagen	Conc. (μM)	Correlation, *r*
Consensus		1.00
Antimycin A (complex III inhibitor)	0.02	0.84
	0.06	0.90
	0.24	0.92
	0.73	0.95
	2.2	0.94
	6.7	0.95
	20	0.95
	60	0.89
Fenpyroximate (complex I inhibitor)	0.02	0.87
	2.2	0.92
	6.7	0.82
	20	0.78
	60	0.80
Pyridaben (complex I inhibitor)	0.02	0.87
	0.1	0.74
	0.3	0.86
	2	0.92
	5	0.73
Rotenone (complex I inhibitor)	0.02	0.88
	0.09	0.86
	0.33	0.94
	1	0.97
	3	0.87
	5	0.85
Valinomycin (ionophore)	0.24	0.91
	0.73	0.91
	2.2	0.83
	6.7	0.88
	20	0.84
	60	0.81

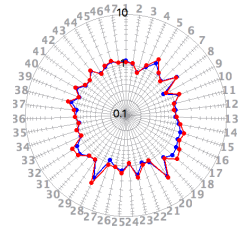

Rotenone (1 μM) *r* = 0.97

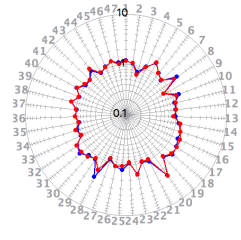

Antimycin A (0.7 μM) *r* = 0.95

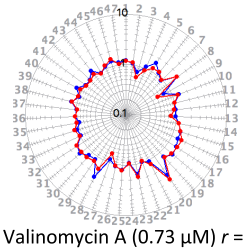

Valinomycin A (0.73 μM) *r* = 0.91

B UPP inhibitors

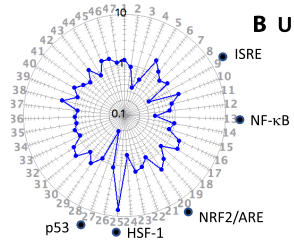

Consensus TFAP

Perturbagen	Conc. (μM)	Correlation, *r*
Consensus		1.00
AM-114 (PS inhibitor)	3.3	0.94
	6.7	0.89
	10	0.80
b-AP15 (deubiquitinase inhibitor)	0.74	0.90
Bortezomib (PS inhibitor)	0.03	0.98
	0.08	0.97
	0.27	0.97
	0.82	0.97
	2	0.96
Lactacystin (PS inhibitor)	3	0.82
	10	0.90
MG-132 (PS inhibitor)	0.08	0.87
	0.74	0.99
	2.2	0.99
	6.7	0.96
	20	0.97
NSC697923 (Ub-conjugating enzyme E2 inhibitor)	2.2	0.69
	6.7	0.71
PSI (PS inhibitor)	6.7	0.95
	20	0.95
	60	0.94
PYR-41 (Ub-activating enzyme E1 inhibitor)	20	0.89
WP1130 (deubiquitinase inhibitor)	2.2	0.84

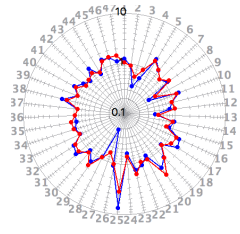

PYR-41 (20 μM) *r* = 0.89

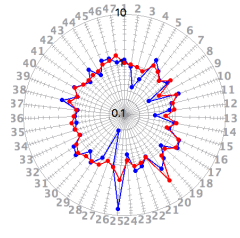

NSC697923 (6.7 μM) *r* = 0.71

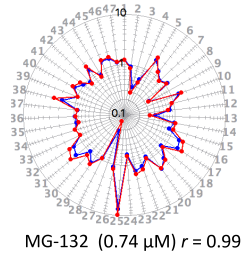

MG-132 (0.74 μM) *r* = 0.99

C TFAPs' endpoints

RTU #	Name
1	TGFRE
2	HNF6
3	TCF
4	Ebox
5	PPAR
6	NF1
7	GR
8	AP-1
9	ISRE
10	MTF-1
11	STAT3
12	TAL
13	NF-κB
14	FoxA2
15	CMV
16	Xbp1
17	CREB
18	AhR
19	EGR
20	NRF2
21	TA
22	ER
23	Oct
24	LXR
25	HSF-1
26	SREBP
27	p53
28	BMPRE
29	Pax6
30	HIF-1α
31	VDR
32	ROR
33	Ets
34	GLI-1
35	NRF1
36	GATA
37	E2F
38	C/EBP
39	Myb
40	PBREM
41	FXR
42	AP-2
43	RAR
44	FoxO
45	SOX
46	Sp1
47	Myc

Fig. 2. The invariant TFAP signatures for inhibitors of mitochondria function and proteasomal degradation. Assay cells (HepG2) were incubated for 24 hours with inhibitors of the mETC or the UPP. Each TFAP signature represents the average data of three independent FACTORIAL assays. The consensus TFAPs of mETC and UPP inhibitors were calculated by clustering the TFAPs of individual perturbagens, as described in Materials and Methods. (**A**) Representative TFAP signatures of mETC inhibitors. (**B**) Representative TFAP signatures of UPP inhibitors. Tables A and B show the similarity values *r* for the TFAPs of the individual perturbagens versus the consensus TFAPs, calculated as a Pearson correlation coefficient. The radial graphs show TFAPs of perturbagens overlaying the consensus TFAPs. Note that the values of TF changes are plotted in a log scale. (**C**) TFAP endpoints.

in agreement with published data (*16*–*18*). Representative TFAPs of MTDs are also shown in fig. S6 as a heatmap. At the end of a 24-hour incubation and the concentrations used, none of the MTDs inhibited cell viability (fig. S4). Therefore, structurally dissimilar MTDs produced an invariant TFAP.

The invariant TFAPs of DNA-damaging agents

To obtain TFAP signatures of DNA damage, we irradiated HepG2 cells by ultraviolet C/ultraviolet B (UVC/UVB) light or treated them with chemicals with different modes of action. Those included topoisomerase I inhibitor camptothecin; topoisomerase II poison auramine O; DNA cross-linking chemicals oxaliplatin, cisplatin, and mitomycin C; and antimetabolites 5-fluorouracil and 5-fluorodeoxyuridine (Fig. 4A). Cluster analysis revealed two distinct TFAP clusters with a low similarity of consensus signatures (*r* = 0.52; Fig. 4, B and C). One cluster had the TFAPs for a low dose of UV irradiation and the chemicals at low concentrations ("a weak DNA damage cluster"; Fig. 4B). The characteristic features of the consensus TFAP were an activation of AP-1, CMV, and p53 RTUs. The other cluster contained the TFAPs for higher UV doses and high concentrations of chemicals ("strong DNA damage"). The consensus TFAP showed multiple responses [including activation of AhR, TCF/β-catenin, and interferon-stimulated response element (ISRE)] and down-regulation of liver X receptor (LXR) (Fig. 4C). Representative TFAPs of the DNA-damaging agents are also shown by the heatmap in fig. S6. Some of these TF responses to DNA damage (for example, p53, AP-1, and AhR) are well known (*19*–*21*). Therefore, the low and high doses of DNA-damaging agents produced two different TFAPs. 5-Fluorouracil and floxuridine elicited only the weak-damage TFAP, while auramine elicited only the strong-damage TFAP at all tested concentrations (Fig. 4A).

The DNA-damaging agents had disparate effects on cell viability; at the end of incubation (24 hours), only some of the treatments (the

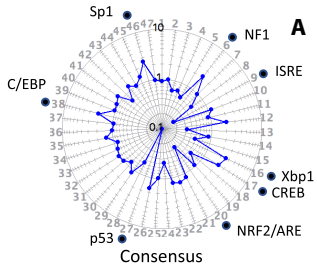

A HDAC Inhibitors

Perturbagen	Conc. (μM)	Correlation, *r*
Consensus		1.00
Apicidin	0.02	0.81
	0.2	0.94
	2	0.97
CAY10398	2	0.96
	20	0.99
KD 5710	2	0.89
	20	0.97
M 344	0.2	0.93
	2	0.97
Oxamflatin	2	0.91
	20	0.94
Pyroxamide	2	0.93
	20	0.97
SAHA	0.3	0.86
	0.8	0.95
	2.5	0.95
	7.4	0.92
	22	0.92
	67	0.93
SBHA	2	0.76
	20	0.96

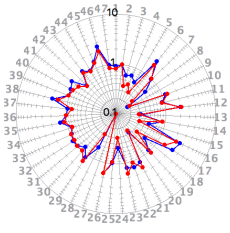
Apicidin (0.2 μM) *r* = 0.94

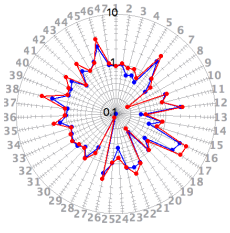
KD 5170 (20 μM) *r* = 0.97

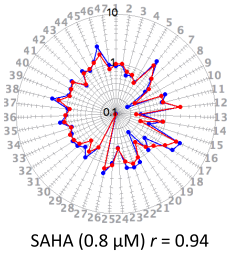
SAHA (0.8 μM) *r* = 0.94

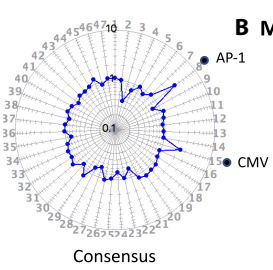

B Microtubule disruptors

Perturbagen	Conc. (μM)	Correlation, *r*
Consensus		1.00
Colchicine	0.08	0.84
	0.25	0.93
	0.74	0.94
	2.20	0.99
	6.70	0.93
	20.00	0.93
	60.00	0.88
Nocodazole	0.74	0.93
	2.20	0.94
	6.70	0.92
	20.00	0.83
	60.00	0.78
Vinblastine	2.20	0.97
	6.70	0.95
	20.00	0.89
	60.00	0.77
Vincristine	6.70	0.95
	20.00	0.95
	60.00	0.93
Vinorelbine	0.25	0.88
	0.74	0.87
	2.22	0.91
	6.67	0.94
	20.00	0.94

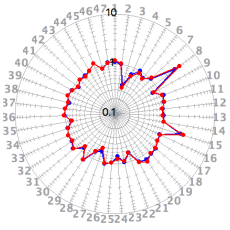
Colchicine (2.2 μM) *r* = 0.99

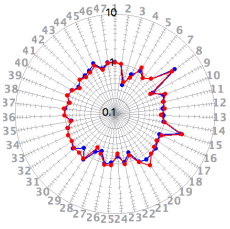
Nocodazole (2.2 μM) *r* = 0.94

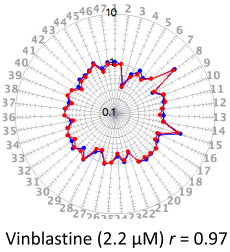
Vinblastine (2.2 μM) *r* = 0.97

C TFAPs' endpoints

RTU #	Name
1	TGFRE
2	HNF6
3	TCF
4	Ebox
5	PPAR
6	NF1
7	GR
8	AP-1
9	ISRE
10	MTF-1
11	STAT3
12	TAL
13	NF-κB
14	FoxA2
15	CMV
16	Xbp1
17	CREB
18	AhR
19	EGR
20	NRF2
21	TA
22	ER
23	Oct
24	LXR
25	HSF-1
26	SREBP
27	p53
28	BMPRE
29	Pax6
30	HIF-1α
31	VDR
32	ROR
33	Ets
34	GLI-1
35	NRF1
36	GATA
37	E2F
38	C/EBP
39	Myb
40	PBREM
41	FXR
42	AP-2
43	RAR
44	FoxO
45	SOX
46	Sp1
47	Myc

Fig. 3. The invariant TFAP signatures for HDAC inhibitors and cytoskeleton disruptors. Assay cells (HepG2) were incubated with HDAC inhibitors or MTDs for 24 hours. Each TFAP represents the average data of three independent FACTORIAL assays. The consensus TFAPs were calculated by clustering those of individual perturbagens, as described in Materials and Methods. (**A**) Representative TFAP signatures of HDAC inhibitors. (**B**) Representative TFAP signatures of MTDs. Tables A and B show the similarity values *r* for the TFAPs of perturbagens at indicated concentrations versus the consensus TFAPs, calculated as a Pearson correlation coefficient *r*. Note that the values of TF changes are plotted in a log scale. The radial graphs show TFAPs of perturbagens overlaying the consensus TFAPs. (**C**) TFAP endpoints.

highest doses of UV and cisplatin) had significantly reduced cell numbers, indicating that the cytotoxicity cannot account for the common TF responses (fig. S5). The fact that DNA-damaging agents produced two distinct TFAPs is consistent with the known biphasic phenotypic response to DNA damage, in which low-level, repairable damage causes a transient arrest of DNA replication, whereas more extensive damage induces permanent arrest of replication (*22*).

In summary, the assessment of specific perturbagens of various cell systems and biological pathways showed that each class of perturbagens had a distinct TFAP. Moreover, perturbagens of the same pathway produced an invariant TFAP, regardless of where and how they interfered.

The invariant TFAP signatures enable identification of compounds with specified bioactivity

The finding of the invariant TFAPs suggested that these signatures could be used to identify chemicals with specific bioactivities among uncharacterized compounds. To test this assumption, we queried a data set of TFAP signatures for the environmental chemicals evaluated by Attagene under the U.S. Environmental Protection Agency (EPA) Toxicity Forecaster (ToxCast) project. These chemicals were screened at multiple concentrations using the FACTORIAL assay in HepG2 cells (*5*, *23*). The ToxCast chemicals were also independently evaluated by other groups using different assays. A Tox21 group has screened this collection for mitochondria inhibitors using a mitochondria membrane potential (MMP) assay, also in HepG2 cells (*24*). The MMP assay data can be found in the EPA Aggregated Computational Toxicology Resource (ACToR) database (*25*). Using these data, we compared the assessments of mitochondria perturbagens using the invariant mETC TFAP and the functional assay.

The ACToR database has data on 2793 ToxCast chemicals that were evaluated by both the MMP and FACTORIAL assays. Of those, the MMP assay scored 518 compounds as mitochondria inhibitors (Fig. 5A). Querying signatures of these 2793 chemicals by the invariant mETC

A DNA-damaging agents

DNA damage weak		
Perturbagen	Conc. (μM)	Similarity, *r*
Consensus		1.00
5-Fluorouracil	0.25	0.69
	0.74	0.77
	2.20	0.82
	6.70	0.91
	20.00	0.95
	60.00	0.95
	133.00	0.91
	200.00	0.81
Camptothecin	1.00	0.65
Cisplatin	20.00	0.76
Floxuridine	6.67	0.76
	20.00	0.82
	60.00	0.79
Mitomycin C	2.20	0.68
	6.70	0.78
	20.00	0.84
Oxaliplatin	0.82	0.86
	2.47	0.87
	7.41	0.81
	22.00	0.82
	66.67	0.68
UV-C	0.8 mJ/cm²	0.72

DNA damage strong		
Consensus		1.00
Auramine	0.09	0.84
	0.27	0.88
	0.82	0.90
	2.47	0.91
	7.41	0.89
	22.22	0.83
Camptothecin	2.20	0.90
	5.00	0.82
	6.70	0.91
	20.00	0.91
	60.00	0.88
Cisplatin	60.00	0.79
Mitomycin C	30	0.78
UV-C	2.4 mJ/cm²	0.90
	4.8 mJ/cm²	0.91

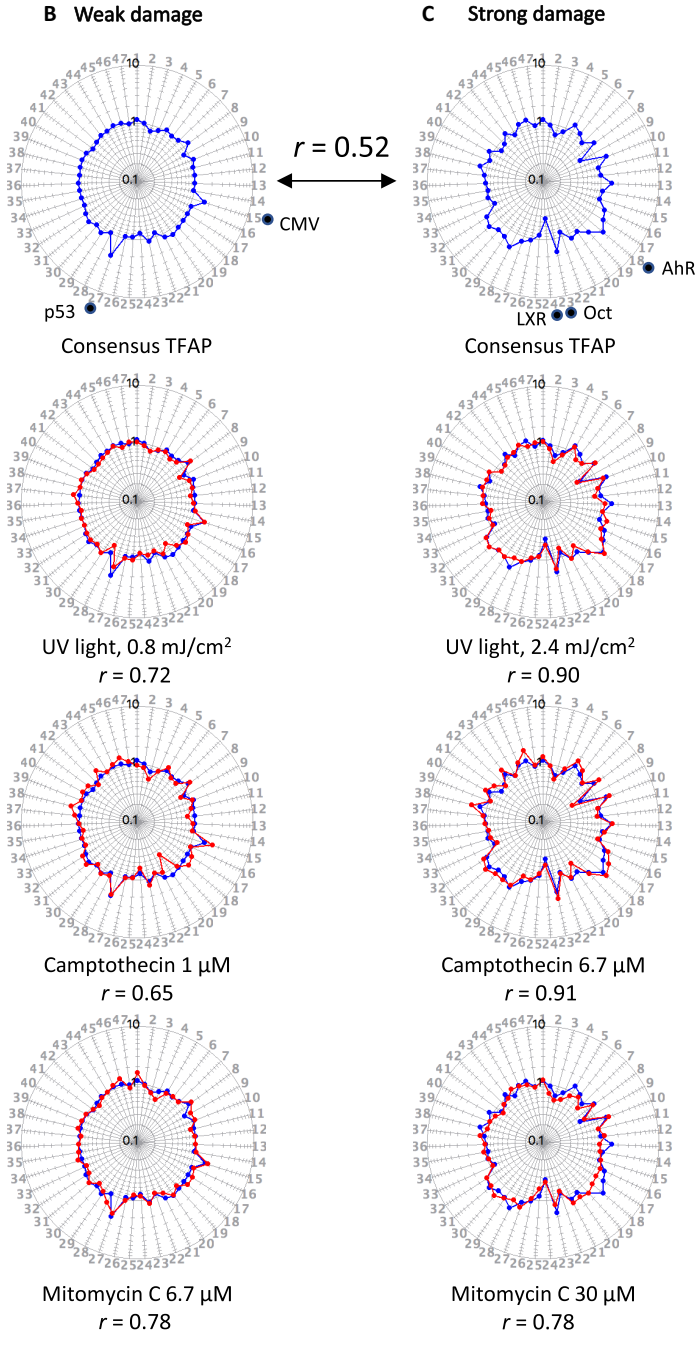

D TFAPs' endpoints

RTU #	Name
1	TGFRE
2	HNF6
3	TCF
4	Ebox
5	PPAR
6	NF1
7	GR
8	AP-1
9	ISRE
10	MTF-1
11	STAT3
12	TAL
13	NF-κB
14	FoxA2
15	CMV
16	Xbp1
17	CREB
18	AhR
19	EGR
20	NRF2
21	TA
22	ER
23	Oct
24	LXR
25	HSF-1
26	SREBP
27	p53
28	BMPRE
29	Pax6
30	HIF-1α
31	VDR
32	ROR
33	Ets
34	GLI-1
35	NRF1
36	GATA
37	E2F
38	C/EBP
39	Myb
40	PBREM
41	FXR
42	AP-2
43	RAR
44	FoxO
45	SOX
46	Sp1
47	Myc

Fig. 4. Low and high doses of DNA-damaging agents produce distinct TFAP signatures. Assay cells (HepG2) were irradiated by a UV source or treated with the indicated chemicals and harvested at 24 hours after the treatments. Each TFAP represents the average data of three independent FACTORIAL assays. The clustering of TFAPs revealed two clusters for the treatments inducing weak and strong DNA damage. (**A**) The table shows the similarity values *r* for the TFAPs of perturbagens at the indicated concentrations versus the TFAPs of the consensus clusters, calculated as a Pearson correlation coefficient. (**B** and **C**) The radial graphs show representative TFAPs of perturbagens overlaying the consensus TFAPs. Note that the values of TF changes are plotted in a log scale. (**D**) TFAP endpoints.

TFAP retrieved a large number of chemicals. For some chemicals, we retrieved multiple TFAPs at different concentrations. To avoid redundancy, we counted each chemical only once.

The concordance of the assays' data was calculated as the percentage of MMP-positive chemicals among the retrieved chemicals. The concordance rate correlated with the TFAP similarity threshold. For example, ~69% of retrieved chemicals with a similarity of $r \geq 0.900$ were MMP-positive. The chemicals with similarity values within $0.800 \geq r \geq 0.700$ had a concordance rate of ~42% (Fig. 5A, middle panel). Representative retrieved signatures are shown in Fig. 5B (top panel).

As we found a significant fraction of MMP negatives among the retrieved chemicals, we searched the literature for retrieved chemicals with high similarity values. With the similarity threshold at 0.800, we retrieved 199 chemicals (listed in table S1). Of those, 118 were

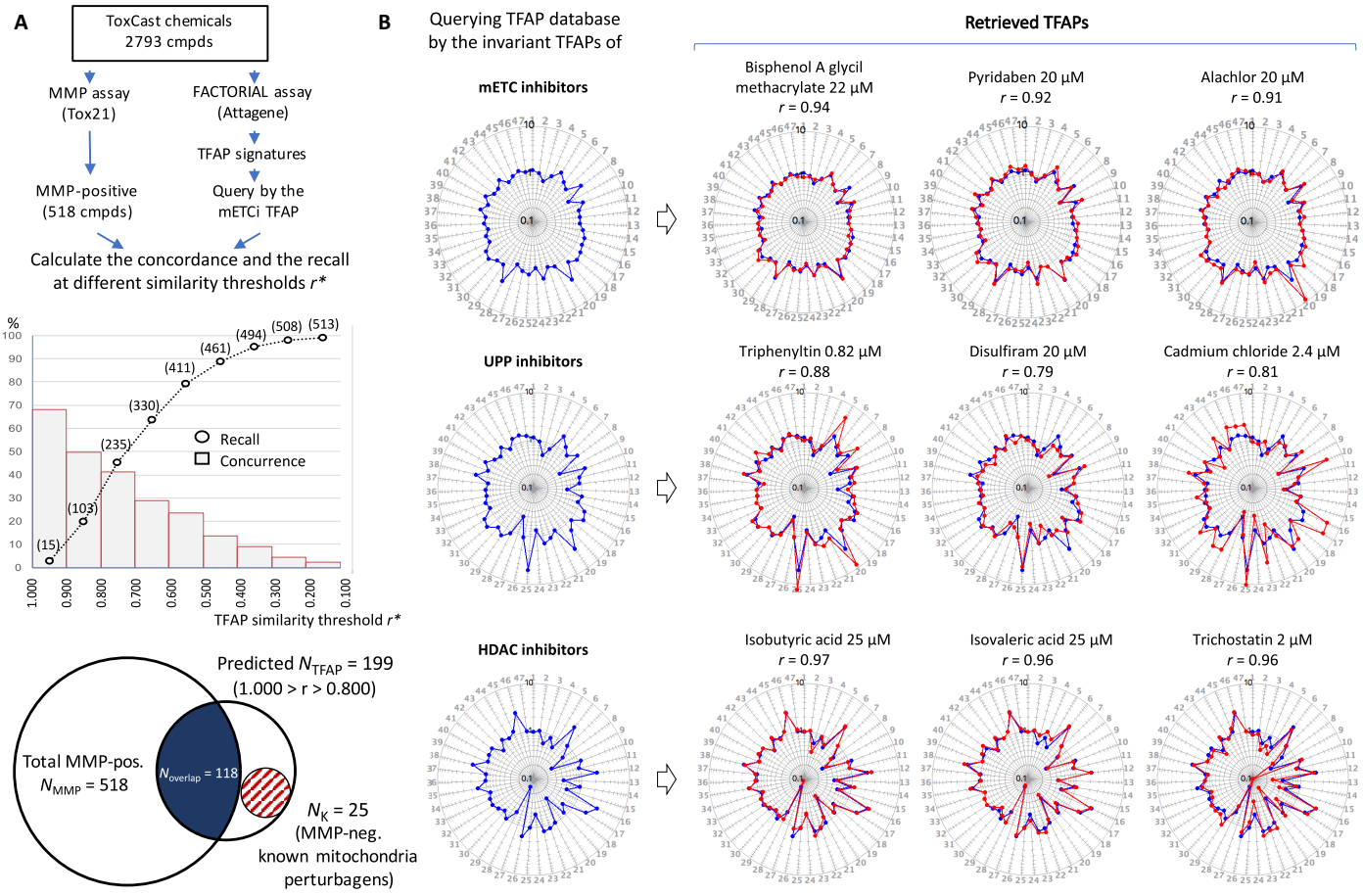

Fig. 5. The invariant TFAP signatures enable the identification of compounds with specified bioactivities. (**A**) Comparing the TFAP-based prediction of mitochondria inhibitors with the data by a functional assay. Top: A total of 2793 ToxCast chemicals was assessed by MMP and FACTORIAL assays. Five hundred eighteen chemicals were scored as mitochondria inhibitors by the MMP assay. The data set of TFAP signatures was queried by the consensus mETC TFAP. The middle panel shows the recall of MMP-positive chemicals (circles) and the concordance rates (bars) for the two assays. The concordance rate is the fraction of MMP positives among the retrieved chemicals that had TFAP similarity values r within the indicated intervals ($r^*_1 \geq r \geq r^*_2$). The cumulative recall curve shows the percentage of 518 MMP positives that were retrieved at different thresholds ($r \geq r^*$). Bottom: The scaled Venn diagram illustrates the relationship between the two assays. The left area represents 518 MMP-positive chemicals. The right area represents the 199 chemicals with TFAP similarity values $r \geq 0.800$ (for the list of retrieved chemicals, see table S1). The intersection area represents the 118 retrieved chemicals that were MMP-positive [concordance of ~59% (118 of 199); recall of ~23% (118 of 518)]. The striped area represents the 25 mETC inhibitors known by the literature that were scored negative by the MMP assay but positive by the FACTORIAL assay (see also fig. S7). (**B**) Querying the TFAP data set by the consensus TFAPs of mETC, UPP, and HDAC inhibitors resulted in retrieved compounds with corresponding bioactivities. Graphs show the similarity of the retrieved and consensus signatures.

MMP-positive, and 81 were MMP-negative (concordance, 59%; Fig. 5A and table S1). The PubMed search showed that at least 25 of the 81 MMP-negative chemicals were known mitochondria disruptors, such as azoxystrobin (*26*) and kresoxim-methyl (*27*). Figure S7 shows the references and representative TFAP signatures for these MMP-negative chemicals. These data indicate that the actual accuracy of TFAP-based predictions was better than we estimated using the MMP assay as a reference. One plausible explanation for this discrepancy is the difference in the screening conditions: We assessed the TFAPs after a 24-hour incubation with concentrations up to 200 µM, whereas the MMP screening entailed a 1-hour incubation at concentrations below 60 µM.

To estimate the cumulative recall of the MMP-positive chemicals, we calculated how many of all 518 MMP-positive chemicals we retrieved by the TFAP query. The recall inversely correlated with the similarity threshold. With a threshold of 0.900, only 15 MMP-positive chemicals were retrieved (~2% recall). The recall increased to ~49% with the threshold set at 0.700 and to 98% with the threshold of 0.200 (Fig. 5A, middle panel). Thus, setting a high similarity threshold for the query improved prediction accuracy, whereas lower thresholds facilitated a broader coverage.

We also found that other invariant TFAP signatures enabled the identification of compounds with the specified bioactivities. For example, querying the Attagene data set by the invariant signatures for UPP perturbagens yielded known UPP inhibitors, including an organotin triphenyltin (*28*), the antialcoholism drug disulfiram (*29*), and cadmium chloride (*30*). Akin to that, the query by the HDAC TFAP also retrieved known HDAC inhibitors, including short-chain fatty acids (isobutyric and isovaleric acid) (*31*) and trichostatin (*14*) (Fig. 5B, bottom panel). Therefore, the invariant TFAPs afforded the identification of compounds with the specified biological activities.

The TFAPs enable the assessment of multiple bioactivities of polypharmacological compounds

Assessments of specific perturbagens of the biological pathways showed that these chemicals produced unchanged TFAPs in a broad concentration range (Figs. 2 to 4). However, we found that many ToxCast chemicals elicited different TFAPs at different concentrations. One such example is glitazones, antidiabetic drugs that target the nuclear receptor peroxisome proliferator–activated receptor γ (PPARγ) and modulate gene expression related to lipid storage, cell differentiation, and inflammation (*32*). Glitazones also share another PPARγ-independent activity that affects the mitochondria function (*33*, *34*). Glitazones bind to mitochondrial membranes and specifically inhibit the mitochondrial pyruvate carrier and respiratory function (*35*). The mitochondria malfunction caused by these drugs has been associated with drug-induced liver injury (DILI) (*33*, *36*). Troglitazone produced the most frequent occurrence of hepatotoxic events and was eventually withdrawn from the market (*33*), while pioglitazone and rosiglitazone are still on the market.

Here, we assessed the TFAPs for troglitazone, which is a most-DILI-concern drug, and pioglitazone, a less-DILI-concern drug. The glitazones produced multiple TFAPs at different concentrations (Fig. 6). At low concentrations, both glitazones produced an identical TFAP, which was consistent with their on-target activity (PPAR activation; Fig. 6, A and B, left panel). With increased concentrations, the primary TFAPs of glitazones transformed into different secondary TFAPs, suggesting the influence of off-target drug activities (Fig. 6A). The signature transformation occurred at different concentrations of troglitazone and pioglitazone (20 μM versus 180 μM, respectively; Fig. 6A). With a further increase in concentration (60 μM), the troglitazone TFAP again transformed into a different tertiary signature (Fig. 6A). The highest concentrations of troglitazone (180 μM) caused cell death (Fig. 6A).

The evident similarity of the secondary signatures of troglitazone and pioglitazone suggested that these drugs had the same off-target activity. Querying the Attagene TFAP database showed that the secondary TFAPs were identical to the invariant mETC TFAP ($r > 0.8$; Fig. 6B,

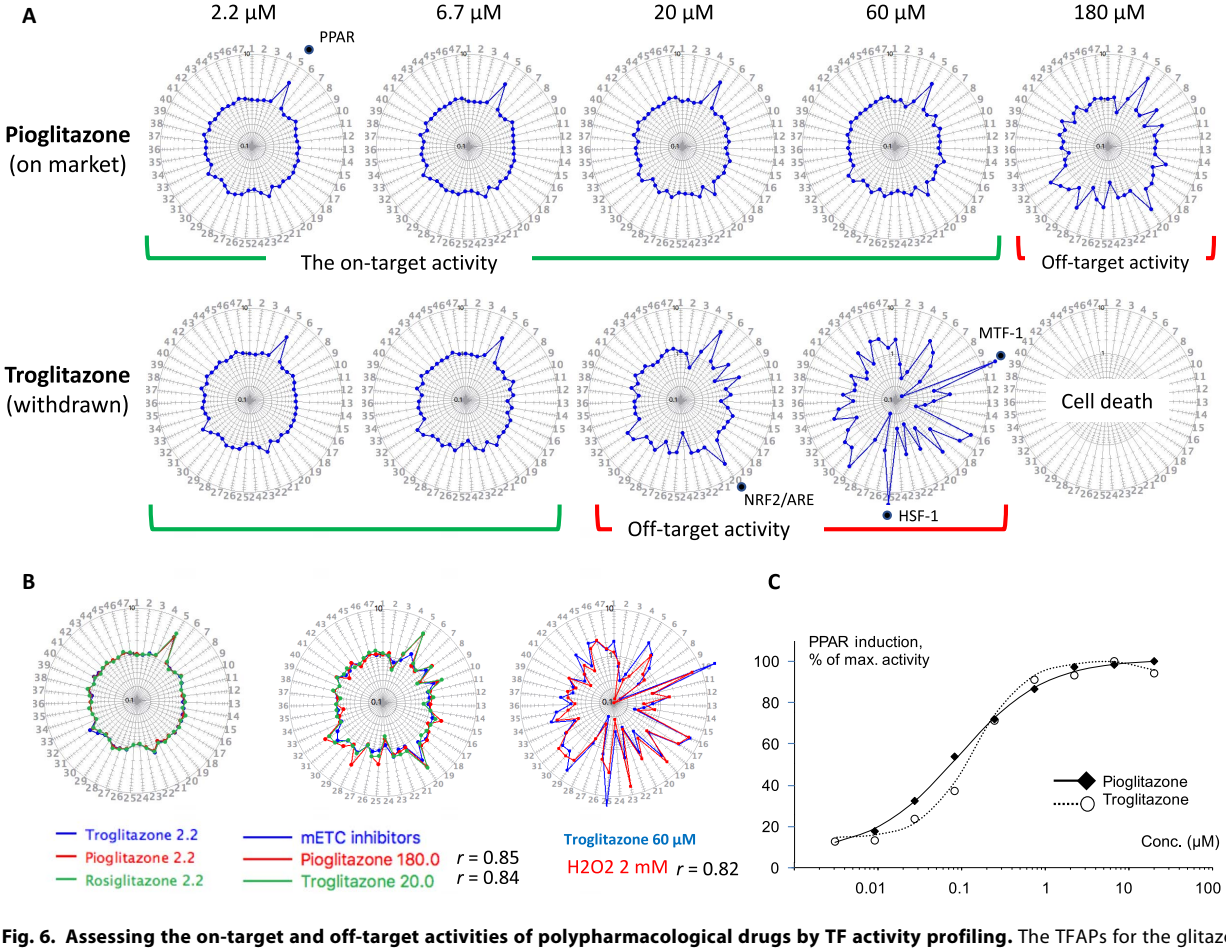

RTU #	Name
1	TGFRE
2	HNF6
3	TCF
4	Ebox
5	PPAR
6	NF1
7	GR
8	AP-1
9	ISRE
10	MTF-1
11	STAT3
12	TAL
13	NF-κB
14	FoxA2
15	CMV
16	Xbp1
17	CREB
18	AhR
19	EGR
20	NRF2
21	TA
22	ER
23	Oct
24	LXR
25	HSF-1
26	SREBP
27	p53
28	BMPRE
29	Pax6
30	HIF-1α
31	VDR
32	ROR
33	Ets
34	GLI-1
35	NRF1
36	GATA
37	E2F
38	C/EBP
39	Myb
40	PBREM
41	FXR
42	AP-2
43	RAR
44	FoxO
45	SOX
46	Sp1
47	Myc

Fig. 6. Assessing the on-target and off-target activities of polypharmacological drugs by TF activity profiling. The TFAPs for the glitazones in HepG2 cells (a 24-hour treatment). Each TFAP represents an average of three signatures by independent FACTORIAL assays. Representative data of the three experiments are shown. (**A**) The TFAP signature transition with increased concentration indicates an influence of off-target drug activities. (**B**) The TFAP signatures enable the identification of the on-target and off-target activities of glitazones. Left: The identical TFAPs for low-concentration glitazones reflect on-target activity (PPAR activation). Middle: Identical secondary TFAPs for pioglitazone and troglitazone at higher concentrations indicate mitochondria malfunction. Right: At the highest concentration (60 μM), the troglitazone TFAP is identical to that of hydrogen peroxide, indicating oxidative stress. (**C**) Assessing dose response of the PPAR RTU to glitazones to determine the AC_{50} values for the on-target activity. Each data point is an average of three independent measurements.

middle panel). Therefore, the secondary TFAPs reflected mitochondria malfunction. Querying the TFAP data set by the TFAP of troglitazone at 60 μM showed high similarity ($r > 0.8$) with the TFAP for hydrogen peroxide (Fig. 6B, right panel). Therefore, high concentrations of troglitazone produced oxidative stress, which is consistent with reports by others (*34*).

Our results show that the assessment of TFAP signatures of glitazones afforded the identification of the primary and off-target activities. The signatures at low concentrations reflected the primary drug activity at PPARγ. The reported AC_{50} (concentration at 50% of maximum activity) values for the PPARγ activation by troglitazone and pioglitazone are of ~200 nM (*37*). These data are consistent with the dose responses of the PPAR RTU to these drugs (Fig. 6C). The secondary TFAP indicated mitochondria malfunction and was consistent with the inhibition of the mitochondrial pyruvate carrier by low micromolar concentrations of glitazones (*35*).

Furthermore, our data may explain the unusually high DILI frequency by troglitazone. The maximum plasma concentrations of troglitazone and pioglitazone in humans are 6.4 and 2.9 μM, respectively. The drugs' TFAPs indicate that these concentrations are below the thresholds for off-target effects (20 and 180 μM for troglitazone and pioglitazone, respectively; Fig. 6A). However, because of variable genetic and environmental factors, it is possible that drug concentration may exceed the mitochondria malfunction threshold in some individuals. As compared to pioglitazone, therapeutic concentrations of troglitazone are much closer to the off-target threshold, increasing the probability of hepatotoxicity. These results demonstrate the utility of TFAP-based assessments for the evaluation of compounds' polypharmacology.

DISCUSSION

Elucidating the biological activity of compounds as relevant to their efficacy and toxicity is an essential objective of biomedical research. In the presented approach, we assessed the bioactivity of compounds by evaluating the responses of signal transduction pathways that regulate gene expression. As a readout, we used the activity of TFs that connect the signaling pathways with the regulated genes. Using the FACTORIAL reporter assay, we characterized cell response by a quantitative signature, the TFAP. A major advantage of the TF activity profiling approach is that it generates simple quantitative signatures that provide clear quantitative metrics to compare the bioactivity of compounds.

The main findings can be summarized as follows: (i) Perturbations of biological pathways/cell systems produce distinct characteristic TFAP signatures; (ii) perturbagens of the same biological pathway elicit an invariant TFAP regardless of where or how they interfere; (iii) the invariant TFAPs enable the identification of compounds with the specified bioactivities among uncharacterized chemicals; and (iv) the assessment of TFAPs of polypharmacological compounds enables the identification of their multiple biological activities.

This approach has clear ramifications for the drug development process. By assessing the TFAP signatures of a chemical, one can identify its potential therapeutic uses and forecast its toxicity. By detecting the transformations of TFAP signatures with varying concentrations, one can compare the off-target activities of drug candidates and the concentration windows wherein the primary activity dominates. This enables a streamlined solution for hit-to-lead selection. Moreover, the TFAP signatures provide insights into drug polypharmacology. While unintended polypharmacology can compromise safety, drugs that modulate multiple disease-relevant targets can be unprecedentedly efficacious. In this regard, the TFAP signatures allow researchers to distinguish between unwanted and desirable polypharmacology. Furthermore, the TFAP assessment enables a straightforward approach to the identification of new indications for approved drugs.

The finding of the invariant TFAPs indicates that disruptions of biological pathways and cell systems cause coordinated changes in the activity of multiple TFs. That implies the existence of specific response programs. As cellular systems operate under permanent pressure from environmental and internal stresses, there must be mechanisms to cope with the possible malfunctions. Some of these mechanisms have been described, such as the retrograde mitochondrial signaling that alters nuclear gene expression to adapt to mitochondria malfunctions (*38*). Another example is the "survival response" that coordinates changes in gene expression to accommodate the global epigenomic disruption by HDAC inhibitors (*39*). In this regard, the invariant TFAP signatures for mETC and HDAC perturbagens (Figs. 2A and 3A) epitomize the signals that regulate these programs.

Here, we have identified the invariant TFAPs for mETC, UPP and HDAC inhibitors, cytoskeleton disruptors, and DNA-damaging agents. This diversity suggests that these invariant signatures should exist for perturbagens of other biological pathways and systems. Our methodology provides the framework for their discovery. Identifying the full complement of these invariant signatures may lead to a new ontology for the bioactivities of compounds.

MATERIALS AND METHODS

Experimental design

Cells and reagents

For the FACTORIAL assay in HepG2 cells [American Type Culture Collection (ATCC) #HB-8065], we used the HG19 subclone (Attagene) that was selected for an elevated xenobiotic metabolic activity (*5*). MCF-7 (ATCC #HTB-22) and HEK293 cells (ATCC #CRL-1573) were from the ATCC. Chemical inhibitors were purchased from Cayman Chemical Company (www.caymanchem.com) and Selleck Chemicals (www.selleckchem.com). The ToxCast chemicals were provided by the ToxCast project (EPA). All chemicals were dissolved in dimethyl sulfoxide (DMSO). The final concentration of DMSO in cell growth medium did not exceed 0.2%.

UV irradiation

Cells were irradiated using a calibrated Spectroline EF-180 UV lamp (Fisher Scientific).

Cell viability

Cell viability was evaluated by the XTT [2,3-bis-(2-methoxy-4-nitro-5-sulfophenyl)-2*H*-tetrazolium-5-carboxanilide] assay (ATCC) in HG19/HepG2 cells. As a baseline, we used cells that were treated with corresponding dilutions of the vehicle (DMSO). The viability data are an average of two replicates. The viability threshold was set at 80% viability.

The FACTORIAL assay

The FACTORIAL assay was reproduced as described (*4*, *5*). The mix of 47 RTU plasmids was transiently transfected in a suspension of assay cells using TransIT-LT1 reagent (Mirus). The transfected cells were plated into 12-well plates. Twenty-four hours later, cells were rinsed and incubated for another 24 hours with the evaluated compounds in a Dulbecco's modified Eagle's medium (DMEM) growth medium supplemented with 1% charcoal-stripped fetal bovine serum and antibiotics. Total RNA was isolated, and the RTU activity profiles were

assessed by consecutive steps of RT-PCR amplification, Hpa I digest, and CE, as described (*5*, *6*).

TFAP signatures

The profile of changes of the transcriptional activity of TFs (the TFAP signature) was calculated by dividing the RTU activity values in compound-treated cells by those in vehicle-treated cells. TFAP signatures were plotted as radial graphs comprising 47 axes showing the fold changes of corresponding RTUs on a logarithmic scale. A value of 1.0 indicated no effects on the TF activity.

Statistical analysis

Assessing the similarity of TFAP signatures

A TFAP signature can be viewed as a vector x in a 47-mer space with coordinates x_i that are log-transformed fold-induction TF values ($\log\Delta TF_i$). The length of the vector is calculated as $|x| = \sqrt{\sum_{i=0}^{47}(\log\Delta TF_i)^2}$. The pairwise similarity of TFAP signatures is calculated as Pearson correlation coefficient r (*5*) that can vary in a range from −1.0 to 1.0.

Calculating the consensus TFAPs for multiple perturbagens

We have modified the average linkage method (*40*) to develop an algorithm for a recurrent agglomerative hierarchical clustering. We start with N clusters $\{C_j\}$, $j = 1$ to N, each containing a single TFAP, to find the clusters $\{C_k\}$ and $\{C_m\}$ with the highest similarity r. These clusters are merged into a $\{C_{km}\}$ cluster. The coordinates of the $\{C_{km}\}$ cluster are calculated as an average of x_k and x_m vectors, taken with the weights equal to the size of clusters N_k and N_m, normalized to their lengths $|x_k|$ and $|x_m|$, and multiplied by the average length of these signatures, as follows

$$x_{km} = \frac{|x_k| \cdot N_k + |x_m| \cdot N_m}{(N_k + N_m)^2} \cdot \left(\frac{x_k}{|x_k|} \cdot N_k + \frac{x_m}{|x_m|} \cdot N_m\right)$$

The resulting TFAP signature was considered as the consensus (average) TFAP for the chemicals within the cluster. The iterative clustering continued until the distance between clusters exceeded a certain similarity threshold r^*. Here, this threshold was set at $r^* = 0.70$.

Comparing the TFAP-based predictions of mitochondria perturbagens with the functional MMP assay data

We queried the data set of TFAPs for ToxCast chemicals using the consensus TFAP for mETC inhibitors (Fig. 2A) and counted the number of retrieved chemicals with similarity values r within certain intervals ($r^*_1 \geq r \geq r^*_2$). The concordance with the MMP assay was calculated as the percentage of MMP-positive chemicals among the retrieved chemicals. To calculate the cumulative recall of the MMP-positive chemicals, we calculated the percentage of the 518 MMP-positive chemicals among the retrieved chemicals at different similarity thresholds.

SUPPLEMENTARY MATERIALS

Supplementary material for this article is available at http://advances.sciencemag.org/cgi/content/full/4/9/eaar4666/DC1

Fig. S1. The effect of mETC inhibitors on the viability of assay cells (HepG2).
Fig. S2. The effect of UPP inhibitors on the viability of assay cells and the common TFAP signatures for UPP inhibitors in HEK293 and MCF-7 cells.
Fig. S3. The common TFAP signatures for HDAC inhibitors in HEK293 and MCF-7 cells and the effect of HDAC inhibitors on the viability of assay cells.
Fig. S4. The effect of MTDs on the viability of assay cells.
Fig. S5. The effect of microtubule DNA-damaging agents on the viability of assay cells.
Fig. S6. An alternative presentation of TF responses to perturbagens as a heatmap.
Fig. S7. The list of known mitochondria disruptors with a high ($r > 0.800$) TFAP similarity to the mETC TFAP that were scored negative by the MMP assay.
Table S1. ToxCast chemicals with a high ($r \geq 0.800$) similarity to the invariant mETC TFAP.
References (*41*–*65*)

REFERENCES AND NOTES

1. J. Lamb, E. D. Crawford, D. Peck, J. W. Modell, I. C. Blat, M. J. Wrobel, J. Lerner, J.-P. Brunet, A. Subramanian, K. N. Ross, M. Reich, H. Hieronymus, G. Wei, S. A. Armstrong, S. J. Haggarty, P. A. Clemons, R. Wei, S. A. Carr, E. S. Lander, T. R. Golub, The Connectivity Map: Using gene-expression signatures to connect small molecules, genes, and disease. *Science* **313**, 1929–1935 (2006).
2. P. Khatri, S. Drăghici, Ontological analysis of gene expression data: Current tools, limitations, and open problems. *Bioinformatics* **21**, 3587–3595 (2005).
3. F. Iorio, R. Bosotti, E. Scacheri, V. Belcastro, P. Mithbaokar, R. Ferriero, L. Murino, R. Tagliaferri, N. Brunetti-Pierri, A. Isacchi, D. di Bernardo, Discovery of drug mode of action and drug repositioning from transcriptional responses. *Proc. Natl. Acad. Sci. U.S.A.* **107**, 14621–14626 (2010).
4. S. Romanov, A. Medvedev, M. Gambarian, N. Poltoratskaya, M. Moeser, L. Medvedeva, M. Gambarian, L. Diatchenko, S. Makarov, Homogeneous reporter system enables quantitative functional assessment of multiple transcription factors. *Nat. Methods* **5**, 253–260 (2008).
5. M. T. Martin, D. J. Dix, R. S. Judson, R. J. Kavlock, D. M. Reif, A. M. Richard, D. M. Rotroff, S. Romanov, A. Medvedev, N. Poltoratskaya, M. Gambarian, M. Moeser, S. S. Makarov, K. A. Houck, Impact of environmental chemicals on key transcription regulators and correlation to toxicity end points within EPA's ToxCast program. *Chem. Res. Toxicol.* **23**, 578–590 (2010).
6. F. Shah, A. Medvedev, A. M. Wassermann, M. Brodney, L. Zhang, S. Makarov, R. V. Stanton, The identification of pivotal transcriptional factors mediating cell responses to drugs with drug-induced liver injury liabilities. *Toxicol. Sci.* **162**, 177–188 (2018).
7. R. Lowry, *Concepts and Applications of Inferential Statistics* (2012); http://vassarstats.net/textbook/ch4apx.html.
8. A. Y. Shih, S. Imbeault, V. Barakauskas, H. Erb, L. Jiang, P. Li, T. H. Murphy, Induction of the Nrf2-driven antioxidant response confers neuroprotection during mitochondrial stress in vivo. *J. Biol. Chem.* **280**, 22925–22936 (2005).
9. L. D. Marroquin, J. Hynes, J. A. Dykens, J. D. Jamieson, Y. Will, Circumventing the Crabtree effect: Replacing media glucose with galactose increases susceptibility of HepG2 cells to mitochondrial toxicants. *Toxicol. Sci.* **97**, 539–547 (2007).
10. A. Ciechanover, Proteolysis: From the lysosome to ubiquitin and the proteasome. *Nat. Rev. Mol. Cell Biol.* **6**, 79–87 (2005).
11. Y. Kawazoe, A. Nakai, M. Tanabe, K. Nagata, Proteasome inhibition leads to the activation of all members of the heat-shock-factor family. *Eur. J. Biochem.* **255**, 356–362 (1998).
12. A. Kobayashi, M. I. Kang, Y. Watai, K. I. Tong, T. Shibata, K. Uchida, M. Yamamoto, Oxidative and electrophilic stresses activate Nrf2 through inhibition of ubiquitination activity of Keap1. *Mol. Cell. Biol.* **26**, 221–229 (2006).
13. M. Haberland, R. L. Montgomery, E. N. Olson, The many roles of histone deacetylases in development and physiology: Implications for disease and therapy. *Nat. Rev. Genet.* **10**, 32–42 (2009).
14. D. C. Drummond, C. O. Noble, D. B. Kirpotin, Z. Guo, G. K. Scott, C. C. Benz, Clinical development of histone deacetylase inhibitors as anticancer agents. *Annu. Rev. Pharmacol. Toxicol.* **45**, 495–528 (2005).
15. G. G. Gundersen, T. A. Cook, Microtubules and signal transduction. *Curr. Opin. Cell Biol.* **11**, 81–94 (1999).
16. T. Akiyama, Y. Kawasaki, Wnt signalling and the actin cytoskeleton. *Oncogene* **25**, 7538–7544 (2006).
17. T.-H. Wang, H.-S. Wang, H. Ichijo, P. Giannakakou, J. S. Foster, T. Fojo, J. Wimalasena, Microtubule-interfering agents activate c-Jun N-terminal kinase/stress-activated protein kinase through both Ras and apoptosis signal-regulating kinase pathways. *J. Biol. Chem.* **273**, 4928–4936 (1998).
18. B. Manavathi, F. Acconcia, S. K. Rayala, R. Kumar, An inherent role of microtubule network in the action of nuclear receptor. *Proc. Natl. Acad. Sci. U.S.A.* **103**, 15981–15986 (2006).
19. A. J. Levine, p53, the cellular gatekeeper for growth and division. *Cell* **88**, 323–331 (1997).
20. E. Shaulian, M. Karin, AP-1 as a regulator of cell life and death. *Nat. Cell Biol.* **4**, E131–E136 (2002).

21. E. Fritsche, C. Schäfer, C. Calles, T. Bernsmann, T. Bernshausen, M. Wurm, U. Hübenthal, J. E. Cline, H. Hajimiragha, P. Schroeder, L.-O. Klotz, A. Rannug, P. Fürst, H. Hanenberg, J. Abel, J. Krutmann, Lightening up the UV response by identification of the arylhydrocarbon receptor as a cytoplasmatic target for ultraviolet B radiation. *Proc. Natl. Acad. Sci. U.S.A.* **104**, 8851–8856 (2007).
22. A. Sancar, L. A. Lindsey-Boltz, K. Ünsal-Kaçmaz, S. Linn, Molecular mechanisms of mammalian DNA repair and the DNA damage checkpoints. *Annu. Rev. Biochem.* **73**, 39–85 (2004).
23. R. Kavlock, K. Chandler, K. Houck, S. Hunter, R. Judson, N. Kleinstreuer, T. Knudsen, M. Martin, S. Padilla, D. Reif, A. Richard, D. Rotroff, N. Sipes, D. Dix, Update on EPA's ToxCast program: Providing high throughput decision support tools for chemical risk management. *Chem. Res. Toxicol.* **25**, 1287–1302 (2012).
24. M. S. Attene-Ramos, R. Huang, S. Michael, K. L. Witt, A. Richard, R. R. Tice, A. Simeonov, C. P. Austin, M. Xia, Profiling of the Tox21 chemical collection for mitochondrial function to identify compounds that acutely decrease mitochondrial membrane potential. *Environ. Health Perspect.* **123**, 49–56 (2015).
25. U.S. Environmental Protection Agency, *EPA ToxCast ACToR Database*; https://actor.epa.gov.
26. A.-H. Gao, Y.-Y. Fu, K.-Z. Zhang, M. Zhang, H.-W. Jiang, L.-X. Fan, F.-J. Nan, C.-G. Yuan, J. Li, Y.-B. Zhou, J.-Y. Li, Azoxystrobin, a mitochondrial complex III Q_o site inhibitor, exerts beneficial metabolic effects in vivo and in vitro. *Biochim. Biophys. Acta* **1840**, 2212–2221 (2014).
27. E. Flampouri, S. Mavrikou, A.-C. Mouzaki-Paxinou, S. Kintzios, Alterations of cellular redox homeostasis in cultured fibroblast-like renal cells upon exposure to low doses of cytochrome bc_1 complex inhibitor kresoxim-methyl. *Biochem. Pharmacol.* **113**, 97–109 (2016).
28. G. Shi, D. Chen, G. Zhai, M. S. Chen, Q. C. Cui, Q. Zhou, B. He, Q. P. Dou, G. Jiang, The proteasome is a molecular target of environmental toxic organotins. *Environ. Health Perspect.* **117**, 379–386 (2009).
29. H. Lövborg, F. Öberg, L. Rickardson, J. Gullbo, P. Nygren, R. Larsson, Inhibition of proteasome activity, nuclear factor-κB translocation and cell survival by the antialcoholism drug disulfiram. *Int. J. Cancer* **118**, 1577–1580 (2006).
30. X. Yu, S. Hong, E. M. Faustman, Cadmium-induced activation of stress signaling pathways, disruption of ubiquitin-dependent protein degradation and apoptosis in primary rat sertoli cell-gonocyte cocultures. *Toxicol. Sci.* **104**, 385–396 (2008).
31. J. Tan, C. McKenzie, M. Potamitis, A. N. Thorburn, C. R. Mackay, L. Macia, The role of short-chain fatty acids in health and disease. *Adv. Immunol.* **121**, 91–119 (2014).
32. E. A. Gale, Lessons from the glitazones: A story of drug development. *Lancet* **357**, 1870–1875 (2001).
33. A. J. Scheen, Hepatotoxicity with thiazolidinediones: Is it a class effect? *Drug Saf.* **24**, 873–888 (2001).
34. D. Hu, C. Q. Wu, Z.-j. Li, Y. Liu, X. Fan, Q.-j. Wang, R.-g. Ding, Characterizing the mechanism of thiazolidinedione-induced hepatotoxicity: An in vitro model in mitochondria. *Toxicol. Appl. Pharmacol.* **284**, 134–141 (2015).
35. A. S. Divakaruni, S. E. Wiley, G. W. Rogers, A. Y. Andreyev, S. Petrosyan, M. Loviscach, E. A. Wall, N. Yadava, A. P. Heuck, D. A. Ferrick, R. R. Henry, W. G. McDonald, J. R. Colca, M. I. Simon, T. P. Ciaraldi, A. N. Murphy, Thiazolidinediones are acute, specific inhibitors of the mitochondrial pyruvate carrier. *Proc. Natl. Acad. Sci. U.S.A.* **110**, 5422–5427 (2013).
36. N. Kaplowitz, Idiosyncratic drug hepatotoxicity. *Nat. Rev. Drug Discov.* **4**, 489–499 (2005).
37. J. Sakamoto, H. Kimura, S. Moriyama, H. Odaka, Y. Momose, Y. Sugiyama, H. Sawada, Activation of human peroxisome proliferator-activated receptor (PPAR) subtypes by pioglitazone. *Biochem. Biophys. Res. Commun.* **278**, 704–711 (2000).
38. Z. Liu, R. A. Butow, Mitochondrial retrograde signaling. *Annu. Rev. Genet.* **40**, 159–185 (2006).
39. J. A. Halsall, N. Turan, M. Wiersma, B. M. Turner, Cells adapt to the epigenomic disruption caused by histone deacetylase inhibitors through a coordinated, chromatin-mediated transcriptional response. *Epigenetics Chromatin* **8**, 29 (2015).
40. P. H. A. Sneath, R. R. Sokal, *Numerical Taxonomy: The Principles and Practice of Numerical Classification* (W. H. Freeman, 1973).
41. L. O. Lim, R. Bortell, A. H. Neims, Nitrofurantoin inhibition of mouse liver mitochondrial respiration involving NAD-linked substrates. *Toxicol. Appl. Pharmacol.* **84**, 493–499 (1986).
42. K. Mihara, N. Isobe, H. Ohkawa, J. Miyamoto, Effects of organophosphorus insecticides on mitochondrial and microsomal functions in the liver of rats with special emphasis on fenitrothion. *J. Pestic. Sci.* **6**, 307–316 (1981).
43. M. A. Tirmenstein, F. A. Nicholls-Grzemski, J.-G. Zhang, M. W. Fariss, Glutathione depletion and the production of reactive oxygen species in isolated hepatocyte suspensions. *Chem. Biol. Interact.* **127**, 201–217 (2000).
44. Q. Saquib, A. A. Al-Khedhairy, M. A. Siddiqui, A. S. Roy, S. Dasgupta, J. Musarrat, Preferential binding of insecticide phorate with sub-domain IIA of human serum albumin induces protein damage and its toxicological significance. *Food Chem. Toxicol.* **49**, 1787–1795 (2011).
45. T. B. Sherer, J. R. Richardson, C. M. Testa, B. B. Seo, A. V. Panov, T. Yagi, A. Matsuno-Yagi, G. W. Miller, J. T. Greenamyre, Mechanism of toxicity of pesticides acting at complex I: Relevance to environmental etiologies of Parkinson's disease. *J. Neurochem.* **100**, 1469–1479 (2007).
46. B. K. Binukumar, A. Bal, R. Kandimalla, A. Sunkaria, K. D. Gill, Mitochondrial energy metabolism impairment and liver dysfunction following chronic exposure to dichlorvos. *Toxicology* **270**, 77–84 (2010).
47. K. J. Cullen, Z. Yang, L. Schumaker, Z. Guo, Mitochondria as a critical target of the chemotheraputic agent cisplatin in head and neck cancer. *J. Bioenerg. Biomembr.* **39**, 43–50 (2007).
48. A. Berson, S. Renault, P. Lettéron, M. A. Robin, B. Fromenty, D. Fau, M. A. Le Bot, C. Riché, A. M. Durand-Schneider, G. Feldmann, D. Pessayre, Uncoupling of rat and human mitochondria: A possible explanation for tacrine-induced liver dysfunction. *Gastroenterology* **110**, 1878–1890 (1996).
49. S. Karami-Mohajeri, M. R. Hadian, S. Fouladdel, E. Azizi, M. H. Ghahramani, R. Hosseini, M. Abdollahi, Mechanisms of muscular electrophysiological and mitochondrial dysfunction following exposure to malathion, an organophosphorus pesticide. *Hum. Exp. Toxicol.* **33**, 251–263 (2014).
50. W. Abdel-Razaq, D. A. Kendall, T. E. Bates, The effects of antidepressants on mitochondrial function in a model cell system and isolated mitochondria. *Neurochem. Res.* **36**, 327–338 (2011).
51. R. A. Videira, M. C. Antunes-Madeira, V. M. C. Madeira, Ethylazinphos interaction with membrane lipid organization induces increase of proton permeability and impairment of mitochondrial bioenergetic functions. *Toxicol. Appl. Pharmacol.* **175**, 209–216 (2001).
52. A. Berson, L. Schmets, C. Fisch, D. Fau, C. Wolf, B. Fromenty, D. Deschamps, D. Pessayre, Inhibition by nilutamide of the mitochondrial respiratory chain and ATP formation. Possible contribution to the adverse effects of this antiandrogen. *J. Pharmacol. Exp. Ther.* **270**, 167–176 (1994).
53. A. E. Dontsov, L. S. Iaguzhinskiĭ, Proton translocation in membranes of submitochondrial particles. *Biokhimiia* **42**, 1123–1127 (1977).
54. H. Schweikl, C. Petzel, C. Bolay, K.-A. Hiller, W. Buchalla, S. Krifka, 2-Hydroxyethyl methacrylate-induced apoptosis through the ATM- and p53-dependent intrinsic mitochondrial pathway. *Biomaterials* **35**, 2890–2904 (2014).
55. R. L. Melnick, C. M. Schiller, Mitochondrial toxicity of phthalate esters. *Environ. Health Perspect.* **45**, 51–56 (1982).
56. J. Usta, S. Kreydiyyeh, K. Bajakian, H. Nakkash-Chmaisse, In vitro effect of eugenol and cinnamaldehyde on membrane potential and respiratory chain complexes in isolated rat liver mitochondria. *Food Chem. Toxicol.* **40**, 935–940 (2002).
57. H. R. Kataria, R. K. Grover, Effect of benomyl and thiophanate-methyl on metabolic activities of Rhizoctonia solani Kühn. *Ann. Microbiol.* **127A**, 297–306 (1976).
58. Q. Saquib, A. A. Al-Khedhairy, B. R. Singh, J. M. Arif, J. Musarrat, Genotoxic fungicide methyl thiophanate as an oxidative stressor inducing 8-oxo-7,8-dihydro-2′-deoxyguanosine adducts in DNA and mutagenesis. *J. Environ. Sci. Health. B* **45**, 40–45 (2010).
59. R. Iorio, A. Castellucci, G. Rossi, B. Cinque, M. G. Cifone, G. Macchiarelli, S. Cecconi, Mancozeb affects mitochondrial activity, redox status and ATP production in mouse granulosa cells. *Toxicol. In Vitro* **30**, 438–445 (2015).
60. M. Baptista, S. J. Publicover, J. Ramalho-Santos, In vitro effects of cationic compounds on functional human sperm parameters. *Fertil. Steril.* **99**, 705–712 (2013).
61. U. Steinfeld, H. Sierotzki, S. Parisi, S. Poirey, U. Gisi, Sensitivity of mitochondrial respiration to different inhibitors in *Venturia inaequalis*. *Pest Manag. Sci.* **57**, 787–796 (2001).
62. G. Schmuck, F. Mihail, Effects of the carbamates fenoxycarb, propamocarb and propoxur on energy supply, glucose utilization and SH-groups in neurons. *Arch. Toxicol.* **78**, 330–337 (2004).
63. G. Grizard, L. Ouchchane, H. Roddier, C. Artonne, B. Sion, M.-P. Vasson, L. Janny, In vitro alachlor effects on reactive oxygen species generation, motility patterns and apoptosis markers in human spermatozoa. *Reprod. Toxicol.* **23**, 55–62 (2007).
64. R. Mesnage, N. Defarge, J. Spiroux de Vendômois, G.-E. Séralini, Major pesticides are more toxic to human cells than their declared active principles. *Biomed Res. Int.* **2014**, 1–8 (2014).
65. T. Yamamoto, S. Terauchi, A. Tachikawa, K. Yamashita, M. Kataoka, H. Terada, Y. Shinohara, Two critical factors affecting the release of mitochondrial cytochrome *c* as revealed by studies using *N,N′*-dicyclohexylcarbodiimide as an atypical inducer of permeability transition. *J. Bioenerg. Biomembr.* **37**, 299–307 (2005).

Acknowledgments: We thank R. Medzhitov and A. Gudkov for helpful suggestions. The views expressed in this publication are those of the authors and do not necessarily reflect the views or policies of the EPA. The mention of trade names does not constitute an endorsement by the EPA. **Funding:** This work was supported by NIH grant R44GM125469. **Author contributions:** A.M. and S.S.M. designed the research. A.M., M.M., L.M., E.M., A.G., L.R., and M.Z. performed the research. S.M. developed algorithms for data analysis.

A.M., K.A.H., S.M., and S.S.M. analyzed the data. S.S.M. wrote the manuscript with input from A.M. and K.A.H. **Competing interests:** A.M., M.M., L.M., E.M., A.G., L.R., M.Z., and S.S.M. have competing financial interests as Attagene employees and shareholders. A.M. and S.S.M. are inventors on a U.S. patent related to this work (no. 7,700,284, issued on 20 April 2010). The authors declare no other competing interests. **Data and materials availability:** All data needed to evaluate the conclusions in the paper are present in the paper and/or the Supplementary Materials. Additional data related to this paper may be requested from the authors.

Submitted 10 November 2017
Accepted 21 August 2018
Published 26 September 2018
10.1126/sciadv.aar4666

Citation: A. Medvedev, M. Moeser, L. Medvedeva, E. Martsen, A. Granick, L. Raines, M. Zeng, S. Makarov Jr., K. A. Houck, S. S. Makarov, Evaluating biological activity of compounds by transcription factor activity profiling. *Sci. Adv.* **4**, eaar4666 (2018).

Science Advances

Evaluating biological activity of compounds by transcription factor activity profiling

Alexander Medvedev, Matt Moeser, Liubov Medvedeva, Elena Martsen, Alexander Granick, Lydia Raines, Ming Zeng, Sergei Makarov, Jr, Keith A. Houck and Sergei S. Makarov

Sci Adv **4** (9), eaar4666.
DOI: 10.1126/sciadv.aar4666